Indian Journal of Engineering & Materials Sciences
Vol. 10, October 2003, pp. 403-412

Characterizing transition metal perovskites with PAC spectroscopy

R Dogra[a*] & A C Junqueira[b]

[a] Beant College of Engineering & Technology, P.O. Box 13, Gurdaspur 143 521, India

[b]Instituto de Pesquisas Energéticas e Nucleares, IPEN-CNEN/SP, P.O. Box 11049, 05422-970 São Paulo, Brazil

Received 21 February 2003; accepted 25 July 2003

Among the several experimental techniques based on different principles available to investigate the materials, the microscopic techniques based on hyperfine interaction form a subclass that characterizes a material at the smallest possible atomic scale. After an introduction to the basic properties of the transition metal perovskites of type ABO_3, the hyperfine interactions along with hyperfine technique such as Perturbed Angular Correlation (PAC) have been briefly described in this paper. The characteristics of the materials analyzed have been expressed in terms of internal magnetic hyperfine fields, electric field gradients and the microscopic point symmetry at the probe site. In particular in this review, a special attention has been paid to the information that can be obtained from a PAC spectroscopy applied to perovskite materials, which may help to understand the microscopic nature of different physical environments around the probe nucleus.

While the fever of superconductivity is still not over, the transition metal oxides of type ABO_3 (A= mostly light rare earths and Ca, Ba, Sr, Bi, Pb, Li; B= transition metals) with perovskite structures again disturbed the whole scientific community with a new surprising and fascinating structural, magnetic and electronic properties (e.g. coupling of spins, charge ordering, metal-insulator transitions, low-spin to high-spin transitions, giant-magneto-resistance and Colossal-magneto-resistance). In particular, the perovskite oxides have been intensively investigated in the recent past because of their extensive use as material for inter-connector of solid oxide fuel cells, IR detector, piezoelectric transducers, electrodes for magneto-hydrodynamic power generators, refractory conducting materials, conducting leads for ZrO_2 based heating elements, ferro-electric memory devices and thin film multi-layer capacitors. So far, a definitive agreement does not exist on the mechanism that give rise to the origin of all these vast number of properties in the perovskites, the studies carried through until the moment relate many of these properties mainly to the variations of crystalline structures of these materials and, coupling between B(*nd*) and O(2*p*) orbitals.

Although the ideal perovskite structure is cubic with largest A cations located at the center of each unit cell, B cations occupying the eight vertices of the cell and the oxygen anions at the center of each edge of the unit cell forming two sublattices: A and BO_6 (see Fig. 1a), the archetypal cubic symmetry is rarely encountered. The ideal cubic structure is distorted by cation size mismatch and Jahn-Teller effect, whereby a distortion of oxygen octahedron surrounding the B cation splits the energy level of a '*d*' ion into triply degenerate $t_{2g}(d_{xy}, d_{yz}, d_{zx})$ and doubly degenerate $e_g(d_{z^2}$ and $d_{x^2-y^2})$ levels, thus lowering the energy. The magnitude of distortion depends upon the ionic size and bond character of the mixed oxide. For the distorted perovskite systems of type ABO_3, a certain

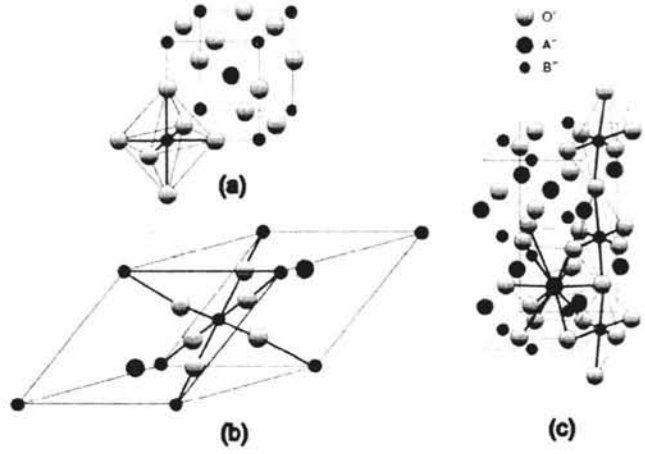

Fig. 1—(a) The basic cubic structural unit of perovskites of type ABO_3 with larger cation A lies at center, the smaller cations B at eight corners and non-metallic anions O at midpoints of cube edges, (b) distorted rhombohedral crystal structure and (c) distorted orthorhombic crystal structure.

*For correspondence (E-mail: drdogra@yahoo.com)

tolerance of fulfilling of the unit cell for ions of different sizes[1] can be expressed as $t = \frac{(r_A + r_O)}{\sqrt{2}(r_B + r_O)}$, where r_A, r_B and r_O are the ionic radii of the elements A, B and O respectively. This factor possesses unitary value for ions of ideal size in a cubic structure. However, perovskites structures could still occur for values in interval $0.89 < t < 1.02(9)$. A $t < 1$ places the $r_B + r_O$ bonds under compression and the $r_A + r_O$ bonds under tension while $t > 1$ does the opposite. Nature accommodates only a $t < 1$ by a cooperative rotation of the corner shared BO_6 octahedra and results into a lowering of symmetry. The distorted structures (see Fig. 1) are usually orthorhombic and rhombohedral (sometimes tetragonal also) that result into different properties of these materials.

Depending on the transition metal ion, perovskites exhibit either localized or collective behaviour of *d*-electrons. The main effect of the various *d*-ions at B position is to vary the number of electrons in the *d*-band and to alter the inter-atomic distances and bond angles, leading to different electrical as well as magnetic properties[2]. For $LaBO_3$ (B=Ti, V, ... , Cu) perovskite series (this series of perovskite materials will be under consideration), the relative size of La^{3+} to BO_6 octahedron is too small to make a cubic structure. The BO_6 octahedron rotates to make some of the distances of La-O bonds shorter. Rotations about at [111] axis reduce the symmetry from cubic to rhombohedral, about a [110] to orthorhombic and about [001] to tetragonal[3]. Moreover, the La-O and B-O bonds have different thermal expansion coefficients and different compressibilities, which suggests that the perovskites structures are dependent on both temperature and pressure. Also the valence of cation A changes the valence of transition metal ion and thus leads to unusual magnetic and electronic properties. Thus, to understand deeply the mechanism that give rise to the origin of these properties in the perovskites, it becomes necessary to disclose details on microscopic scale if some suitable microscopic technique using appropriate probes at A and B sites is available.

The hyperfine interaction studies, which have received a distinguished recognition in solid state material research, provides information on the local environment by observing magnetic and electric hyperfine interactions. The measurements like heat capacities, electric and magnetic susceptibilities, neutron and X-ray diffraction derived parameters in perovskite materials represent only gross averages over the atomic scale properties of these materials. It is the hyperfine spectroscopy, which probes the strength and symmetry of the local crystal fields at the microscopic scale. The basic principles of the technique involve interaction of the nuclear electromagnetic moments (electric-quadrupole moment Q and magnetic-dipole moment μ) with the electromagnetic fields (electric field gradient EFG and magnetic hyperfine field MHF) arising from the extra-nuclear electronic charge and spin distributions in the crystal lattice. The hyperfine interaction measurements in solids directly give corresponding electromagnetic coupling energy of the nucleus, namely (i) electric quadrupole interaction, and (ii) magnetic hyperfine interaction.

Several techniques [Mössbauer effect (ME), nuclear orientation (NO), nuclear magnetic resonance (NMR), nuclear quadrupole resonance (NQR), electron spin resonance (ESR) and perturbed angular correlation/distribution (PAC/PAD)], which partly compete and partly complement, have been utilized for the measurements of these hyperfine interactions. Because of several advantages (like temperature insensitive, smaller impurity-impurity interactions) of perturbed angular correlation technique over others, it is better suited to follow phenomena as a function of temperature (many perovskites show magnetic ordering and phase transition phenomena at high temperature). Moreover, the perturbed angular correlation technique has been successfully applied in the past decades to investigate electrically ordered and magnetically ordered perovskite materials[4-8]. Basically, this technique is based on the correlation between emission directions of two successive radiations emitted during a nuclear decay cascade and thus, the method requires an introduction of radioactive probe nuclei into a specific site in the crystal lattice of interest and subsequently measuring the hyperfine interactions at those sites. For practical reasons (e.g. concerning radiochemistry, anisotropic γ–γ cascade population, the half-life of the intermediate level, nuclear electromagnetic moments of the intermediate state), the most favourable PAC probes at present are very few and are summarized in Table 1 along with their useful nuclear properties.

Table 1—Properties of PAC probe nuclei. $T_{1/2}$, I, $t_{1/2}$, Q, μ, A_{22} respectively represent the half life of parent nuclei, intermediate spin, half life of intermediate spin level I, quadrupole moment intermediate level I, magnetic moment of intermediate level I and anisotropy of the γ–γ cascade under consideration

Probe	$T_{1/2}$	I	$t_{1/2}$ (ns)	γ–γ (keV)	Q (b)	$\lvert\mu\rvert$ (μ_N)	$\lvert A_{22}\rvert$ (%)	Production
$^{44}Ti \xrightarrow{EC} {}^{44}Sc$	48 y	1^-	153	78-68	0.18	0.344	4.5	^{45}Sc(p,2n)^{44}Ti
$^{99}Mo \xrightarrow{\beta^-} {}^{99}Tc$	67 h	$5/2^+$	3.6	740-181	-	3.291	10	^{98}Mo(n,γ)^{99}Mo
$^{99}Rh \xrightarrow{EC} {}^{99}Ru$	16 d	$3/2^+$	20.5	528-90	0.23	0.284	22	^{99}Ru(d,2n)^{99}Rh
$^{100}Pd \xrightarrow{EC} {}^{100}Rh$	3.6 d	2^+	215	84-75	0.076	4.324	16	^{103}Rh(p,4n)^{100}Pd
$^{111}Ag \xrightarrow{\beta^-} {}^{111}Cd$	7.5 d	$5/2^+$	84.5	95-247	0.83	0.765	13	^{110}Pd(n,γ)^{111}Pd
$^{111}In \xrightarrow{EC} {}^{111}Cd$	2.8 d	$5/2^+$	84.5	173-247	0.83	0.765	18	^{109}Ag(α,2n)^{111}In
$^{111m}Cd \rightarrow {}^{111}Cd$	49 m	$5/2^+$	84.5	95-247	0.83	0.765	16	^{110}Cd(n,γ)^{111m}Cd
$^{133}Ba \xrightarrow{EC} {}^{133}Cs$	10.5 y	$5/2^+$	6.3	356-81	0.33	3.45	3.6	^{132}Ba(n,γ)^{133}Ba
$^{140}La \xrightarrow{\beta^-} {}^{140}Ce$	40 h	4^+	3.5	329-487	0.1	4.35	13	^{139}La(n,γ)^{140}La
$^{172}Lu \xrightarrow{EC} {}^{172}Yb$	6.7 d	2^+	1.8	1095-79	2.16	0.67	38	^{172}Yb(p,n)^{172}Lu
		3^+	8.3	91-1095	2.87	0.65		
$^{181}Hf \xrightarrow{\beta^-} {}^{181}Ta$	42 d	$5/2^+$	10.8	133-482	2.35	2.57	23	^{180}Hf(n,γ)^{181}Hf
$^{187}W \xrightarrow{\beta^-} {}^{187}$Re	24 h	$9/2^-$	554	480-134	3.3	5.11	12	^{186}W(n,γ)^{187}W

A more detailed description of the PAC technique can be found elsewhere[9-10]. A typical PAC set-up is shown in the Fig. 2. After the emission of first γ-ray, the nucleus starts to live in an intermediate state with spin direction $\vec{I}(t=0)$ and during this time the nuclear electromagnetic moments (Q or μ) interact with the hyperfine fields (MHF or EFG) at the probe nucleus. This interaction causes the probe nucleus to reorient and to emit a second γ-ray in a direction different than if no hyperfine field is present at the probe nucleus and, the spin changes to direction $\vec{I}(t=\Delta t)$ after time Δt through an angle $\Delta\theta$. In a semi-classical picture, this effect is known as precession of the nuclear spin around the direction of the hyperfine field with precession frequency proportional to $\Delta\theta/\Delta t$ which results from the torque originated by hyperfine fields acting on the electromagnetic moments. This measurable effect

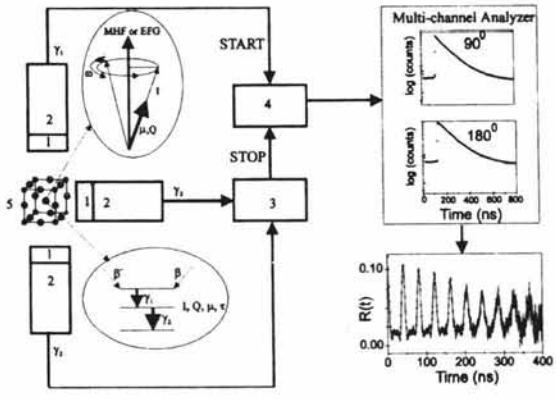

Fig. 2—A typical PAC set-up showing the radioactive probe nucleus sitting in the host lattice. (Upper in-set showing the precession of the electromagnetic moments around the hyperfine field, and lower in-set showing the γ–γ cascade with intermediate state having lifetime τ_N, electric quadrupole moment Q and magnetic dipole moment μ [(1) BaF_2/NaI scintillators, (2) PMT, (3) OR gate, (4) time to amplitude converter and (5) sample with probe])

perturbs the spatial angular correlation of the γ-rays and forms a basis for PAC spectroscopy.

In practice, PAC measurements are sensitive to both electric quadrupole interactions and magnetic hyperfine interactions. The static electric quadrupole interactions provide a measure of the strength and symmetry of the crystal field in the vicinity of the probe nucleus. In this case, since the vibrational motion of the atoms in the lattice is very rapid relative to the PAC timescale, the measured EFG appears to arise from the time-averaged positions of the atoms, and the sharpness of the spectral lines reflects the "motional narrowing" effect. In contrast to static interactions, time-varying interactions arise when the EFG fluctuates during the intermediate-state lifetime. These interactions provide information about defect and ionic transport. The effect of the fluctuating EFG is to destroy the orientation of the intermediate level which appears as attenuation of the angular correlation. On the other hand, the magnetic hyperfine interactions, which can be measured in ferromagnetic/ antiferromagnetic and paramagnetic materials, are used to study the effects of defects and lattice distortions in materials that have cubic symmetry. The general approach is to measure the magnetic hyperfine interaction in a material with few defects. The cubic symmetry requires that the electric quadrupole interaction vanish. When either defects or distortions are produced, a quadrupole interaction arises that attenuates the usually well-defined magnetic interactions, the analysis of which can provide information about the type of defect that produced the quadrupole interaction.

Since the hyperfine fields are dominated by contributions from electronic charges and spins within the first few atomic distances around the probe atom, the more distant charges and spins only contribute to in-homogeneous broadening of signals, the precession frequencies can be used to characterize the different local atomic environments around the probe atoms. Once such a frequency has been identified with an underlying environment, it can be utilized to study the following phenomena: (i) phase transformations: multiphase analysis, (ii) structural and magnetic phase transitions: critical behaviour and exponents, (iii) magnetism: spin dynamics, stability of atomic magnetic moments in different hosts, exchange interactions, thin film and multilayered structures, (iv) surfaces and interfaces: nano-materials, and (v) point defects: their types, properties, interactions, radiation and implantation damage and hydrogen trapping at defect sites in metals.

It has been learned through past experience in different types of materials that (a) if the charge distribution around the probe nucleus has cubic symmetry, the EFG is zero, (b) if the charge distribution around the probe nucleus has axially symmetric environment (e.g. trigonal, hexagonal and tetragonal), the EFG is non-zero and asymmetry parameter is zero, (c) if probe nucleus has surroundings of lower symmetry (e.g. orthorhombic, monoclinic, triclinic), both EFG and asymmetry parameter are non-zero, and (d) besides, a probe nucleus symmetrically surrounded by neighbours with anti-ferromagnetically coupled magnetic moments will probably feel a zero or small hyperfine field, whereas ferromagnetically coupled surroundings will give considerably higher value.

Thus, the transition metal perovskites, which exhibit variety of structures, offer very good candidates to investigate these observations through PAC technique, which is highly sensitive to local structure variations.

Experimental Procedure

PAC probe chemistry

It is the probe atoms that play a very decisive role in the PAC experiments. The major problem in these experiments is that of sample preparation, that is mainly doping of host material with probe atoms, without changing the properties of the host metals. The PAC experiments can be performed with radioactive probe atoms at concentrations much lower than 1 ppm. To dope a material with the radioactive probe atoms, following procedures can be used: (i) implantation of accelerated radioactive ions into the sample, (ii) thermal treatment of the sample, so that the probe atoms are introduced via diffusion or melting, and (iii) through chemical reaction.

The advantage of the first procedure is its applicability to all isotopes even in the case of low solubility of probes atoms into host, e.g., alkali metals in rare-earths or vice versa. With the help of sufficiently high implantation energies, the surface layers of the metal can be easily overcome. Second procedure leads to well-defined metallurgical state of the impurity in the respective metal. The third procedure is well suited to metal-oxides (e.g.

delafossite ABO_2, perovskites ABO_3, and ferrites AB_2O_4), which can be prepared through chemical reaction (citrate gel process, co-precipitation and complex compound process) and during sample preparation, the required quantity of radioactive probe can be added. The radioactive material is homogeneously distributed in the sample and this homogeneity is usually retained even after sintering at very high temperature. A detailed description of the perovskite sample preparation through chemical route is described elsewhere[11].

PAC set-up and data acquisition

The typical three detectors PAC set-up is shown in Fig. 2, where the crystalline sample containing radioactive probe nuclei is placed at the center of the detectors assembly. The start and stop gamma rays, are detected by the scintillation detectors coupled to photo-multiplier tubes, are fed to the time-to-amplitude converter (TAC). Before feeding start and stop signals to TAC, the signals are properly corrected with the help of electronic module, differential constant fraction discrimination (DCFD). Using DCFD, the contribution from noise signals, X-rays and unwanted gamma rays can be minimized. The multi-channel analyzer records the time intervals between start and stop gamma rays, known as time distribution of nuclear lifetimes. The recorded time distribution is a lifetime decay curve modulated by the spin precessions of the nucleus by the extranuclear fields known as internal fields (magnetic hyperfine fields or electric field gradient). Measuring these time distribution curves will provide information about the internal fields present in the sample. To keep the sample at desired temperature, a specially designed tubular furnace of diameter about 3-4 cm is installed at the center of the detectors geometry. Since the smaller detector-sample distance reduces the prompt contribution in the time distribution curve, the conical scintillators are being widely used to achieve the same.

PAC measurements and analysis

Experimentally, the primary quantity measured in the PAC experiment is the time distribution $W(\theta,t)$ of γ-rays in the γ–γ cascade populating intermediate level I and can be obtained by recording the coincidence counting rate when succeeding γ-ray is detected at time t after the first γ–ray detection at an angle θ. The coincidences are generally recorded at desired temperatures using a standard set-up of BaF_2/NaI(Tl) detectors arranged in a planar 90°-180° geometry which has a time resolution of 0.6 ns/1.0 ns corresponding to 511 keV annihilation gamma rays of ^{22}Na radioactive source. For polycrystalline samples, the time distribution function $W(\theta,t)$ can be written as an expansion of Legendre polynomial $P_k(\cos\theta)$,

$$W(\theta,t) = \exp(-t/\tau_N)[1 + A_{22}G_{22}(t)P_2(\cos\theta) + A_{44}G_{44}(t)P_4(\cos\theta)] \quad \ldots (1)$$

where time independent terms A_{kk} (k=2,4) denote the anisotropy coefficients which contain the spatial correlation information of the γ–γ cascade involved. The time dependent functions $G_{22}(t)$ and $G_{44}(t)$ depend on the nature of the extra-nuclear fields and contain all the desired information about the hyperfine interaction of the probe ion with its environment. In most of the cases, as $A_{44} >> A_{22}$, the higher order terms in above expression are neglected. The exponential decay factor takes into account the radioactive decay of the intermediate level having lifetime τ_N. The numerical reduction of these distributions removes the effects of exponential decay and provides the desired experimental quantity known as spin rotation or perturbation function $R(t)$ that shows the effects of modulation and is given by:

$$R(t) = 2.\frac{[C(180°,t) - C(90°,t)]}{[C(180°,t) + 2C(90°,t)]},$$

where $C(\theta,t)$ are the geometric mean of the coincidences taken from the spectra recorded at angles 180° and 90° respectively. In the paramagnetic phase of the material, the measured perturbation function $R(t)$ are fitted with the suitable model for the static nuclear electric quadrupole interaction:

$$R(t) = A_{22}G_{22}(t) = A_{22}\sum_i f_i G_{22}^i(t) + C \quad \ldots (2)$$

here f_i are the fractional site populations and C is the time-independent baseline shift (or hard core value) that takes into accounts the effects of γ-rays that are absorbed by the sample en-route to the detectors and the effects of probe nuclei that are not in well-defined chemical environments. $G_{22}^i(t)$ are the corresponding perturbation factors given by:

$$G_{22}(t) = \sum_n S_{2ni}(\eta_i)\cos(\omega_{ni}(\eta_i)t) \times \exp\left(\frac{-(\delta_i\omega_{ni}t)^p}{2}\right).\exp\left(\frac{-(\tau_R\omega_{ni}t)^2}{2}\right) \quad \ldots (3)$$

where the primary frequencies ω_n and their amplitudes S_{2n} are related to the hyperfine splitting of the intermediate nuclear level and depend on the nuclear quadrupole frequency ω_Q and the electric field gradient tensor V_{ij} $(i,j=x,y,z)$, with V as the electrostatic potential at the nuclear site. In the principal axis system of the EFG tensor, only the diagonal components are non-zero and $V_{xx}+V_{yy}+V_{zz}=0$, the EFG is usually expressed in terms of largest component V_{zz}. The non-vanishing component of electric field gradient V_{zz} is related to the quadrupole frequency ω_Q by $\omega_Q = eQV_{zz}/4I(2I-1)\hbar$ and is measured in terms of spin independent quadrupole frequency $\nu_Q = eQV_{zz}/h$ where Q is the nuclear electric quadrupole moment. The quadrupole frequency ν_Q is known as coupling constant that contains the information about the strength of the interaction. The deviation of the EFG from the axial symmetry is given by the asymmetry parameter $\eta = (V_{xx} - V_{yy})/V_{zz}$ with $0 \le \eta \le 1$. For η=0, the perturbation function is harmonic and periodic, and for non-zero value of η, the oscillations in the perturbation function are periodic and non-harmonic.

The detector system should have sufficient time resolution in order to distinguish the different contributions towards observed spin rotation function. The effects of finite time resolution τ_R of detectors and the distribution of EFG with a width δ (p=1 and p=2 respectively represent Lorentzian and Gaussian type distribution) are properly taken into account in Eq. (3). In order to fit the perturbation functions measured in magnetic phase region, a known function for the combined electric and magnetic interaction[10] in a polycrystalline sample can be used from which the quadrupole frequency ν_Q as well as the Larmor frequency $\omega_B = g\,\mu_N B_{hf}/\hbar$ can be deduced, where g is the nuclear g-factor and B_{hf} is the magnetic hyperfine field.

Results and Discussion

In the following, we will discuss the important informations that can be drawn from the PAC measurements in transition metal perovskites.

Site allocations

Since the spin rotation function $R(t)$ is characteristic of a particular surroundings around the probe nucleus, therefore if chemically different surroundings are present in a particular system the measured perturbation function will reflect an abundance of each contribution. Analysis of the observed perturbation function can make possible to separate these different contributions in the system and thus to assign these contributions to a specific positions in the system which will enable to know different occupation of the probe nuclei. The perturbation functions for $LaFeO_3$ and $LaCoO_3$ samples with $^{111}In/^{111}Cd$ probe along with their respective Fourier transforms are shown in Fig. 3, that clearly indicating a superposition of signals from two local environments of the probe nuclei in $LaFeO_3$ and single interaction frequency in $LaCoO_3$ perovskites. The PAC spectra were least square fitted with up to two/three probe sites using theoretical perturbation function given by Eq. (2). It was observed in $LaCrO_3$ and $LaFeO_3$ compounds that the ^{111}Cd probe nuclei prefer to substitute both at La as well as Cr(Fe) sites[11], the higher quadrupole frequency (~140 MHz) was assigned to La site and lower quadrupole frequency (~40 Mz) to Cr(Fe) sites. The observed quadrupole frequency at 295 K (ν_Q ~40.4(1) MHz) in $LaCoO_3$ perovskite is almost identical to those obtained at Cr(Fe) sites in $LaCr(Fe)O_3$ perovskites and therefore, we assign this to the ^{111}Cd probe nuclei substituting the Co atomic sites.

EFG and their distributions

In a defect free crystal where each probe nuclei in the crystal lattice interact with an identical EFG, the measurement of static probe site EFG should yield a sharp spectral lines, i.e., δ should be very small (see Fig. 3). On the other hand, measurements yield broadened lines (i.e. δ is large) when small intrinsic defects (such as point defects, disordered structure or impurities) lie in the neighbourhood of probe ion as each probe nuclei in the lattice interact with somewhat randomly varying EFG. Therefore, this large distribution in EFGs will cause a damping of the amplitudes of spin rotation pattern with increasing time. Fig. 4 shows the damped PAC spectra for $La_{1-x}Sr_xCoO_3$ perovskite using $^{181}Hf \rightarrow ^{181}Ta$ probe at room temperature. In view of the large number of possible microscopic La-Sr combinations, one should expect a broad distribution in spin rotation pattern of electric quadrupole interaction leading to a strong damping. Thus, the analysis of electric quadrupole interaction in disordered materials will give hyperfine parameters that would mask the actual values.

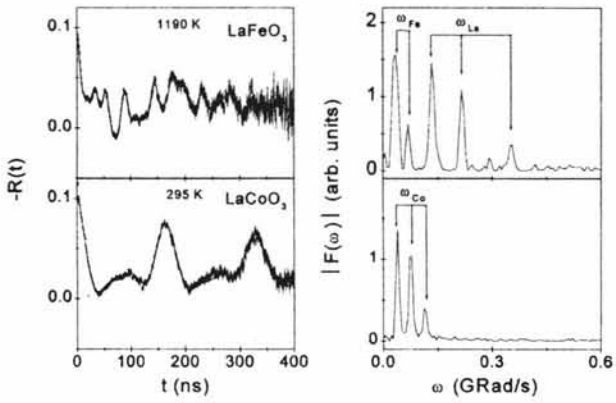

Fig. 3—The perturbation functions and their Fourier transforms for ^{111}Cd probes in $LaFeO_3$ (from ref. 11) and $LaCoO_3$ perovskites at indicated temperatures (Solid lines are the least squares fit of the appropriate theoretical function to the experimental data. ω_{La}, ω_{Fe} and ω_{Co} indicate the frequency components assigned to the different probe sites in the samples, and sharp lines in the Fourier spectra clearly indicate the probe site is defect free)

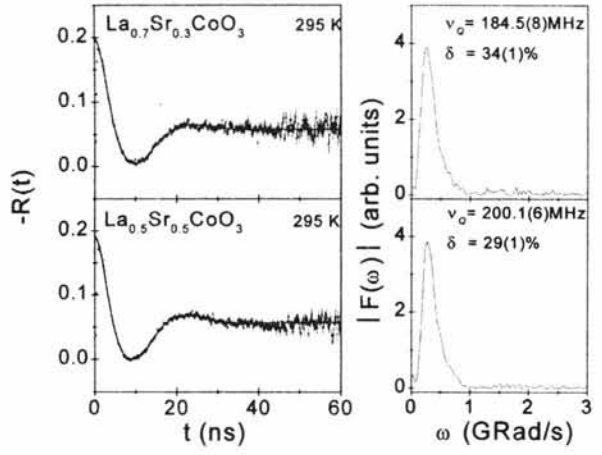

Fig. 4—The perturbation functions and their Fourier transforms for ^{111}Ta probes in $La_{1-x}Sr_xCoO_3$ perovskites at room temperature (Solid lines are the least squares fit of the appropriate theoretical function to the experimental data for one site model and the damped spectra indicate that the all probe nuclei are not observing the same EFG which in turn reflect as broaden lines in the Fourier spectra)

Magnetic hyperfine field

Fig. 5a represents the spin rotation pattern for antiferromagnetically ordered perovskite $LaFeO_3$ using $^{111}In \rightarrow ^{111}Cd$ PAC probe where magnetic hyperfine field for ^{111}Cd nucleus at Fe site is observed along with electric quadrupole interaction[11]. The observed magnetic hyperfine field at ^{111}Cd probe nuclei is coming from the transfer of spin density from paramagnetic Fe^{3+} ions to the diamagnetic Cd^{2+} ion through Fe^{3+}-O^{2-}-Cd^{2+} bonds. The transfer occurs

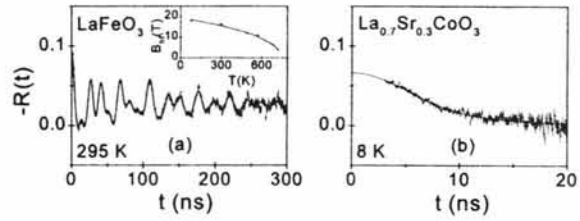

Fig. 5—The perturbation functions for ^{111}Cd and ^{140}Ce probes respectively in $LaFeO_3$ (from ref. 11) and $La_{0.7}Sr_{0.3}CoO_3$ perovskites below their Neel temperatures. Spectrum (a) was fitted with a two sites model of combined electric quadrupole and magnetic dipole interaction while spectrum (b) was fitted with a model for magnetic interaction only (The in-set shows the Power law variation of magnetic hyperfine field ($B_{hf}(T) = B_{hf}(0)(1 - T/T_N)^{\beta}$ with β=0.44 (2) for ^{111}Cd probe at Fe site in $LaFeO_3$ as a function of temperature)

through the spin polarization of the closed Cd^{2+} s-shells by magnetic neighbours as well as through the overlap of the oxygen *p*-orbital transferring unpaired spin density into the outermost Cd 5*s*-orbital. Although $LaCoO_3$ perovskite is non-magnetic even at very low temperature, doped sample ($La_{1-x}Sr_xCoO_3$; $0.1<x<1$) possesses localized itinerant ferromagnetism. Fig. 5b shows the PAC pattern obtained with $^{140}La \rightarrow ^{140}Ce$ probe at 8 K in $La_{0.7}Sr_{0.3}CoO_3$, showing a very slow interaction frequency. Since the quadrupole moment of the 2083 keV 4^+ state of ^{140}Ce is known to be very small, we expect the observed interaction is only due to pure magnetic dipole interaction at the La site. The observed magnetic hyperfine field at La site in $La_{0.7}Sr_{0.3}CoO_3$ compound is small ~1.8(2)T, as relatively small spin density is likely to be transferred to Ce ion at La site from the nearest Co^{3+} ions. This is due to the fact that the Co^{3+}-O^{2-}-La^{3+} exchange bond angle is approximately 90° and produces a very small overlap of oxygen orbitals with orbitals of cerium.

Local point symmetry and phase transitions

Since the PAC spectroscopy usually involves impurity atoms, which generally differ in size or charge from the atoms of the host material, the measured hyperfine parameters may differ from the one measured using identical probe-host atom combination. That is why Mössbauer and PAC measurements give quite different results for the same material studied. But at the same time these size and charge differences are important when PAC technique is applied to characterize point defects in the materials, as probe atoms can trap vacancies and

interstitials. The presence of these point defects in the neighbourhood of the probe breaks the local point symmetry of the crystal lattice, which in turn generates an EFG at the probe site and this EFG differs in magnitude and symmetry from the probe site EFG generated by perfect crystal lattice. Analysis of the temperature dependence of the hyperfine parameters can provide useful information concerning defects trapping, their diffusion and formation energies. Moreover, the EFG sensed by PAC probe nuclei represent the local point symmetry about the probe and not necessarily the overall symmetry of the crystal. Consequently, PAC can be used to follow the changes on the microscopic scale, when new micro-surroundings at the probe site will start appearing such as change of bond distances, change of symmetry and trapping of defects, causing changes in the EFG value. An example of phase transition mechanism studied by PAC technique in perovskite materials is shown in Fig. 6, yielded information about the orthorhombic-to-rhombohedral phase transition in $LaCrO_3$, where co-existence of two different type of grains has been observed[11]. The observed decrease in the asymmetry parameter η to nearly zero and an increase in the EFG values for the ^{111}Cd probe nuclei at La and Cr sites near structural phase transition temperature provide the microscopic evidence that the local point symmetry of the crystal has changed. A similar trend of hyperfine parameters has also been observed in $LaFeO_3$[11] and $LaMnO_3$[12] perovskites with ^{111}Cd and ^{181}Ta probe nuclei respectively. Furthermore, a linear temperature dependence of coupling constant ν_Q at Co site in $LaCoO_3$ perovskite with $^{111}In \rightarrow {}^{111}Cd$ and $^{181}Hf \rightarrow {}^{181}Ta$ probes (see Fig. 7) has ruled out the possibility of symmetry change around temperature 600 K, in contrast to the observed one with other techniques. It is, therefore, apparent that the PAC technique can be used as a powerful tool (phase detector) for establishing crystallographic phase transitions in the materials. Moreover, a linear temperature dependence of EFG at transition metal site with ^{111}Cd probe in rhombohedrally distorted perovskites $LaBO_3$ (B=Cr,Fe,Co) has been observed, indicating the strong dependence of the EFG on local oxygen coordination[14,15]. This linear temperature dependence of EFG seems to indicate microscopic evidence for slight positional changes of the ions in the crystal lattice with temperature. Not only this, the observed temperature dependence of EFG in $LaCoO_3$ perovskite has also shown the thermally induced spin transition of Co^{3+} ion from low-spin $t_{2g}^6 e_g^0$ ground state configuration to high-spin $t_{2g}^4 e_g^2$ state[13].

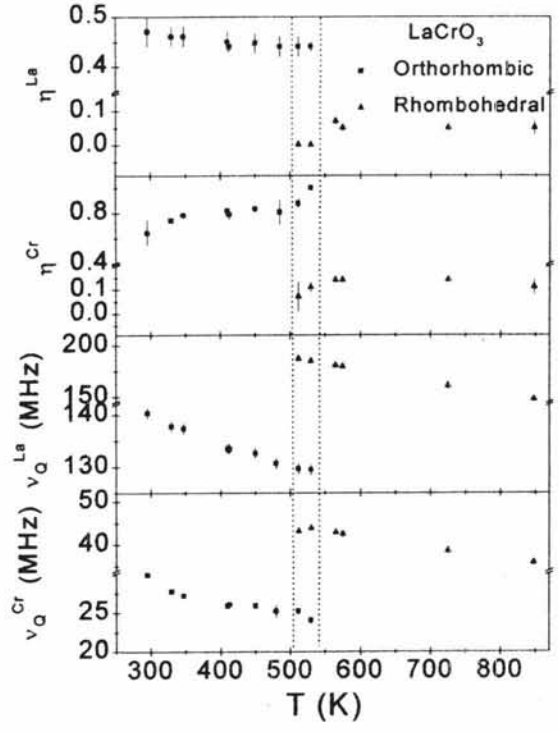

Fig. 6—Temperature dependence of fitted hyperfine parameters for ^{111}Cd at La and Cr sites in $LaCrO_3$ (The dotted lines show the region of the coexistence of both orthorhombic and rhombohedral phases[11])

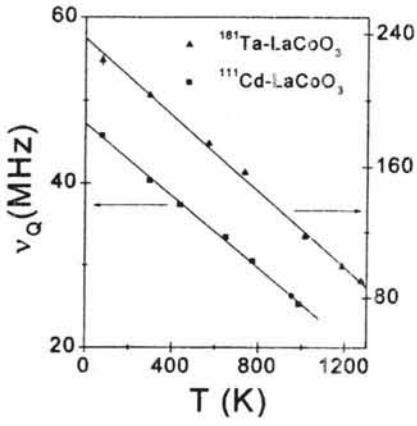

Fig. 7—Temperature dependence of measured coupling constant ν_Q at Co site in $LaCoO_3$ perovskite with ^{111}Cd and ^{181}Ta probes (from ref. 11) (The solid lines in the figure represent a least square fit of a function $\nu_Q(T) = \nu_Q(0)(1 - CT)$ to the data points, with constants C(Cd)=4.95(5)×10^{-4} MHz/K and C(Ta)=5.19(5)×10^{-4} MHz/K)

Covalent character of B-O bonds in $LaBO_3$ (B = Cr, Mn, Fe, Co) perovskites

The hyperfine fields at the site of interest in solids arise from the electrons (the bonding electrons, the conduction electrons and local electronic shells of the probe ion) near the nucleus. The rest of the charges in the material produce the electrostatic potential at the nuclear site that determines the electron densities. It is, therefore, evident that for calculating components of electric field gradients, we must know the total electron wave functions. The charges outside the probe nuclei generate an electric field gradient which make polarization of the local electronic shells with contribution $(1-\gamma_\infty)V_{zz}^{latt}$, where γ_∞ is known as Sternheimer antishielding factor with $10 \le -\gamma_\infty \le 80$. For atoms with unfilled, non-spherical electronic shells (e.g. rare earths ions) an additional local electric field gradient V_{zz}^{loc} is created and modified by a factor R $(-0.2 \le R \le 0.2)$, therefore, total EFG at the site of interest is $V_{zz}^{tot} = (1-\gamma_\infty)V_{zz}^{latt} + (1-R)V_{zz}^{loc}$. This model, generally known as Point Charge Model (PCM), offers a very good approximation in many ionic crystals and some insulators, it will thus be interesting to see whether this will work equally in the perovskites also and can be used to conclude about the ionic nature of the crystal.

The PCM calculations of V_{zz} and η were performed for both cation sites in these transition metal perovskites. Formal charges of +3 and –2 were assigned to La, Cr, Mn, Fe, Co and oxygen ions respectively. The lattice sum was performed numerically to within a sphere of radius of 100 Å with probe atom at the origin. The lattice parameters and the atomic positions were taken from the Rietveld analysis of the samples. The resulting value of V_{zz}^{latt} was then multiplied by $(1-\gamma_\infty)$ to obtain the value of EFG at the nuclear site, $V_{zz}^{PCM} = (1-\gamma_\infty)V_{zz}^{latt}$. The results of the PCM calculation of V_{zz} and η are summarized in Table 2 for La and Cr/Mn//Fe/Co sites in $LaBO_3$ (B=Cr, Mn, Fe, Co) perovskites. The experimental results are included in this table for comparison purpose. While the agreement between the experimental and calculated values of asymmetry parameters η is reasonable only for the La sites, the agreement for V_{zz} is quite poor. The discrepancy between the experimental and PCM values can be associated with the incomplete description of the EFG involved in PCM calculations, where the local contribution to EFG, arising from electronic characteristics of the probe, has not been taken into consideration. In a previous compilation[14] of EFG's for ^{111}Cd probe nuclei at cation sites for different types of oxides, a better agreement between the experimental V_{zz} and V_{zz}^{PCM} was obtained for cases where the cation-O^{2-} bond distances were greater than 2.1Å. In the transition metal perovskites, the La-O^{2-} and B-O^{2-} bond distances range from 2.50 to 2.72 Å and 1.92 to 1.98Å, respectively. Although the disagreement between experimental and calculated EFG values larger in this work, we can conclude that basically a similar behaviour is followed by these compounds. These results imply the strong covalent contribution to EFG at transition metal site in $LaBO_3$ perovskites. Recently, first-principle calculations based upon full-potential-linearized-augmented-plane-wave[15] (FP-LAPW) have been applied successfully to see the influence of Cd impurity in delafossite oxides[16] of type ABO_2, and these

Table 2—Experimentally determined room temperature values of η and V_{zz} for the $LaCrO_3$, $LaMnO_3$, $LaFeO_3$ and $LaCoO_3$ perovskites with ^{111}Cd probe nuclei compared with the values calculated by PCM for a distorted crystal structures

Sample	Crystal Structure	PAC Probe Utilized	Probe Nuclei at Sites	η	V_{zz} (10^{21}V/m^2)	η^{PCM}	$\lvert V_{zz}^{PCM} \rvert$ (10^{21}V/m^2)	Remarks
$LaCrO_3$	Orthorhombic	$^{111}In \rightarrow ^{111}Cd$	La	0.47(3)	7.0(9)	0.53	2.5	Ref. [9]
			Cr	0.64(9)	1.5(2)	0.92	23.5	
$LaMnO_3$	Orthorhombic	$^{111}Ag \rightarrow ^{111}Cd$	La	0.56(2)	7.4(1)	0.44	3.46	Present work
			Mn	0.49(2)	3.2(1)	0.42	14.2	
$LaFeO_3$	Orthorhombic	$^{111}In \rightarrow ^{111}Cd$	La	0.43(2)	7.3(9)	0.45	4.2	Ref. [9]
			Fe	0.95(5)	1.3(2)	0.43	16.0	
$LaCoO_3$	Rhombohedral	$^{111}In \rightarrow ^{111}Cd$	La	-	-	0	2.21	Present work
			Co	0	2.0(3)	0	3.1	

calculations have reproduced the experimental results. Thus, such electronic structure calculations may also be required to describe correctly the effects of covalent bonding in perovskites of type ABO_3.

Conclusions

To perform all these measurements in transition metal perovskites, we used crystal chemistry to introduce an appropriate probe into the sites of interest. The following conclusions have been drawn from the PAC measurements: (i) the PAC measurements have shown that $^{111}In/^{111}Cd$ probe nuclei prefer to substitute both La and Cr/Mn/Fe sites in $La(Cr/Mn/Fe)O_3$ perovskites while in $LaCoO_3$ compound it substitute only for Co sites, (ii) in the doped sample $La_{1-x}Sr_xCoO_3$, the static electric quadrupole interactions have shown the line broadening of spectral lines due to different microscopic combinations of La and Sr ions in the lattice, (iii) temperature dependence of hyperfine parameters in these perovskites has shown that the PAC technique can be effectively used for local crystal structure transitions, (iv) the PAC measurements in perovskites can be utilized to measure the supertransferred magnetic hyperfine field. Besides, the PCM calculations of V_{zz} and asymmetry parameter η for ^{111}Cd nuclei substituting the La as well as Cr, Mn, Fe and Co sites were carried out for $LaBO_3$ (B=Cr, Mn, Fe, Co) compounds and prediction has been made about the covalent nature of B-O bond in ABO_3. We hope that the present work (as PAC measurements are very sensitive to electronic structure) in these transition metal perovskites will stimulate further interest among theoreticians to develop a better understanding to correlate effects of 3d-band occupation with the observed electric field gradients and magnetic hyperfine field. Furthermore, the PAC measurements in dimensionally confined thin films of these compounds are in progress that will provide information about the stability of novel structure in thin layers of perovskites.

Acknowledgements

Authors thankfully acknowledge the financial support provided by the Fundação de Amparo para Pesquisa do Estado de São Paulo (FAPESP), Brazil, in the form of a research fellowship.

References

1 Goldschmidt V, *Geochemistry* (Clarendon Press, Oxford), 1958.
2 Hamada N, Sawada H, Solovyev I & Terakura K, *Physica*, B 237 (1997) 11.
3 Goodenough J B, *J Alloys Compounds*, 262 (1997) 1.
4 Catchen G L, Wukitch S J & Saylor E M, *Ferroelectrics*, 117 (1991) 175.
5 Rearick T M, Catchen G L & Adams J M, *Phys Rev*, B 48 (1993) 224.
6 Catchen G L, Hollinger E F & Rearick T M, *Z. Naturforsch*, 51a (1996) 411.
7 Rasera R L & Catchen G L, *Phys Rev*, B 58 (1998) 3218 and references therein.
8 Roth J, Uhrmacher M, Pressa P, Ziegeler L & Lieb K P, *Z Naturforsch*, 55a (2000) 242, and references therein.
9 Frauenfelder H & Steffen R, *Alpha, beta and gamma ray spectroscopy* (North Holland, Amsterdam), 1965, 997.
10 Butz T, *Nuclear spectroscopy and charge density wave systems* (Kluwer Academic, Norwell, MA), 1992, 325; Catchen G L, *Hyp Int*, 88 (1994) 1.
11 Dogra R, Junqueira A C, Saxena R N, Carbonari A W, Mestnik J & Moralles M, *Phys Rev*, B 63 (2001) 224104.
12 Catchen G L, Evenson W E & Allred D, *Phys Rev*, B 54 (1996) R3679.
13 Junqueira A C, Dogra R, Carbonari A W, Saxena R N & Mestnik-Filho J, *Hyp Int*, 136/137 (2001) 509.
14 Carbonari A W, Mestnik-Filho J, Attili R N, Moralles M & Saxena R N, *Hyp Int*, 120/121(1999) 475.
15 Blaha P, Dufeck P, Schwarz K & Haas H, *Hyp Int*, 97/98 (1996) 3 and references therein.
16 Lalic M V, Mestinik-Filho J, Carbonari A W, Saxena R N & Moralles M, *J Phys*, 14 (2002) 5517.